Growth of AlGaN alloys under excess Group III conditions: Formation of Vertical Nanorods

Chirantan Singha, Sayantani Sen, Pallabi Pramanik, Mainak Palit, Alakananda Das, Abhra Shankar Roy, Susanta Sen, Anirban Bhattacharyya

PII: S0022-0248(17)30634-6
DOI: https://doi.org/10.1016/j.jcrysgro.2017.10.027
Reference: CRYS 24347

To appear in: *Journal of Crystal Growth*

Received Date: 5 May 2017
Revised Date: 20 October 2017
Accepted Date: 21 October 2017

Please cite this article as: C. Singha, S. Sen, P. Pramanik, M. Palit, A. Das, A. Shankar Roy, S. Sen, A. Bhattacharyya, Growth of AlGaN alloys under excess Group III conditions: Formation of Vertical Nanorods, *Journal of Crystal Growth* (2017), doi: https://doi.org/10.1016/j.jcrysgro.2017.10.027

Growth of AlGaN alloys under excess Group III conditions: Formation of Vertical Nanorods

Chirantan Singha[a], Sayantani Sen[a], Pallabi Pramanik[a], Mainak Palit[a], Alakananda Das[b], Abhra Shankar Roy[a], Susanta Sen[b], Anirban Bhattacharyya[b*]

[a] *Centre for Research in Nanoscience and Nanotechnology, University of Calcutta, JD2 Sector III Salt Lake City, Kolkata-700106, West Bengal, India*

[b] *Institute of Radio Physics and Electronics, University of Calcutta, 92 A. P. C. Road, Kolkata-700009, West Bengal, India*

Abstract

Droplet Epitaxy of AlGaN nanostructures was investigated in this work. Growth was carried out by Plasma Assisted Molecular Beam Epitaxy (PA-MBE) under extreme group III rich conditions, where the excess metal remained on the growth surface and formed nanoscale metallic droplets due to the interplay of surface energy, surface diffusion and desorption, all of which are strongly dependent on the relative arrival rates of Gallium and Aluminum and the substrate temperature. Intermittent exposure of this metallic film to active nitrogen forms various types of nanostructures, whose morphology, composition and luminescence properties were evaluated. Our results indicate that for AlN, the droplet epitaxy process forms random arrays of uniform well oriented [0001] nanorods with a height of ~1µm and a diameter of 250nm. For AlGaN grown under excess gallium, and intermittent exposure to the active plasma, structures with diameters of 200µm to 600µm and a height of 80nm were observed. We report the spontaneous formation of lateral concentric heterostructures under these conditions. A single photoluminescence (PL) peak was observed at about 260nm with a room temperature to 4K intensity ratio of ~25%.

Keywords: A1. Nanostructures, A3. Molecular Beam Epitaxy, A3. Migration Enhanced Epitaxy, B1. Nitrides

* Tel: +91 9903212063
Corresponding Author: anirban.rpe@caluniv.ac.in (A. Bhattacharyya)

1. Introduction

Field emission devices based on semiconducting materials play a significant role in many applications, ranging from display screens to electron microscopy [1-2]. While optical emitters based on III-Nitride semiconductors [3-5] are well established, these materials are also important candidates for field emission devices [6-7], along with carbon based materials such as diamond microtip arrays or carbon nanotubes [8]. The conduction band of AlN is very close to the vacuum level (~6.12eV), [9] making it an appropriate choice. In addition, the III-Nitrides are technologically advanced, therefore for these materials, the field emission structures can be monolithically integrated into electronic devices and circuits. Furthermore, the high chemical and thermal stability of AlN allows a large current density.

Currently, most of the research on field emission devices is based on vertical nanowire arrays [10], which are expected to significantly decrease the turn-on voltage. AlN vertical nanowires have been grown by several techniques, including arc discharge [3], vapour-solid [4], vapour-liquid-solid [11] as well as epitaxial processes such as Molecular Beam Epitaxy (MBE) [12] and Metal Organic Chemical Vapour Deposition (MOCVD) [13]. However, it is a challenge to generate well oriented structures with relatively uniform height and cross section. Growth of GaN nanostructures have been also reported by various groups, specially on to Silicon substrates [14]. In case of AlGaN nanowires, the increase of AlN mole fraction in the alloy reduces the electron affinity significantly which is desired for field emission, but this increase also typically requires a significantly higher growth temperature for chemical vapour deposition processes.

In this work, growth of high Al content AlGaN alloys and nanostructures have been carried out by the Plasma Assisted Molecular Beam Epitaxy (PA-MBE) technique. The growth of nanostructures by MBE typically is carried out using the Stranski-Krastanov growth method

that is the strain related islanding process [15-17]. However, such structures require the formation of a wetting layer, which may not be appropriate for many applications. Another growth process that has been employed is the "droplet epitaxy", where nearly spherical nanoscale droplets of Gallium, Aluminum or their alloys are formed on the growth surface, which are subsequently nitridated to form nano-dots. This has been studied in depth for GaN, InGaN as well as AlGaN quantum dots [18-21].

Growth of III-Nitrides by the PA-MBE process typically requires high group III content in order to generate smooth surfaces and interfaces. It has been reported previously that growth of AlGaN under weak excess group III conditions lead to nanoscale compositional inhomogeneity, which strongly affect their carrier localization and recombination [21]. In this paper, we investigate very high excess group III conditions of growth, and the formation of various nanostructures due to droplet epitaxy type processes.

2. Experimental Details

All the growths of AlGaN films for this work were carried out using a VEECO Gen-930 (PA-MBE) system, on c-plane single side polished sapphire substrates of 2-inch diameter (MONOCRYSTAL Inc, Russia). Dual filament effusion cells were used as the source of Aluminum (6N5, Azelis) and Gallium (7N, Azelis). An RF plasma source (UNI-Bulb) was employed for nitrogen activation. The nitrogen gas was of 6N5 purity, which was additionally passed through GATEKEEPER® filters to further reduce the impurity level for oxygen and water vapour to less than 100 ppt. Post growth the samples were observed under a LEICA WILD M420 "makroscope". The surface profile was scanned using a BRUKER DektakXT system. A Zeiss Auriga Field Effect Scanning Electron Microscope (FESEM) system was used to study the surface morphology. An INCA Energy 250 Microanalysis System mounted on to an EVO 18 Scanning Electron Microscope (SEM) (Zeiss) was

employed for Energy Dispersive X-ray Spectroscopy (EDX). Photoluminescence (PL) studies were carried out using a 10mW He–Ag laser (Photon Systems) emitting at 224 nm as the excitation source. The samples were mounted on to the cold finger of a 4K cryostat (Cryo-Industries of America) for temperature dependent measurements.

Prior to deposition, the substrate was outgassed initially at over 100ºC to remove moisture, and then mounted on to a heated station placed inside the preparation chamber of the MBE system, and progressively heated to 400ºC, while maintaining a vacuum level of 10^{-9}T. The substrate was then introduced into the growth reactor, and heated to 800ºC while maintaining similar vacuum levels. A clear RHEED pattern was observed from the sapphire substrate at this stage.

Growth was initiated by exposing the substrate to active nitrogen for one hour, using an RF plasma power of 350W. A flow rate of 1.7sccm was maintained for nitrogen, which corresponds to a process chamber pressure of $1.95x10^{-5}$T. The active nitrogen converts the topmost layers of Al_2O_3 to AlN, which act as nucleation centers for the subsequent deposition of an AlN buffer layer.

AlN buffers have been used by various groups for nucleation of III-Nitride growth on to sapphire substrates, both for MBE as well as for MOCVD techniques [22]. For MBE processes, this deposition can be carried out either under nearly stoichiometric conditions, or under excess group III which leads to smoother surfaces. A number of groups have reported a specific deposition technique, where the substrate is exposed sequentially to group III flux and the group V flux, called Migration Enhanced Epitaxy (MEE) [23]. A modified version of this process has been also reported where the active nitrogen is kept constant, and the group III flux was made incident on to the substrate in a switched mode, that is the flux was

on for a period of time T_{on} and then turned off for T_{off} seconds [24-25]. In this paper, the AlN growth was initiated using a similar methodology.

The Al flux employed for the growth of the AlN layer was chosen to be significantly higher than that necessary for stoichiometric deposition. Several optimization growths were carried out, and estimates for the conditions of stoichiometry were established by observation of the RHEED pattern during deposition. The RHEED pattern during deposition of AlN under excess group III becomes dim and diffuse from scattering of the electron beam by a metallic layer present on the growth surface. When the growth is altered by closing the Al shutter, the RHEED transforms from the dim and diffuse to a clear pattern as the Al metal is consumed by the impinging active nitrogen. The time taken for this transformation is an indication of the group III to group V flux ratio, and for nearly stoichiometric conditions, this takes less than 10 seconds. From such observations, the Al flux necessary for stoichiometric growth of AlN using the plasma conditions as mentioned previously, and a substrate temperature of 750^{o}C was found to be 1.45×10^{-7}T. For the growth carried out in this work, a very high Al flux of 2.33×10^{-7}T was employed.

The process of droplet epitaxy of III-Nitrides requires the formation of nanoscale metallic islands on the growth surface, which is subsequently converted into the semiconductor by reaction with active nitrogen [26-27]. This has been reported for GaN where the growth was studied in real time by GISAXS techniques [27]. It was observed by Wang et. al. that the size distribution of the Gallium nanodroplets as measured in real time can be correlated to that of GaN nano-dots as measured post growth. Specifically, both dot size and dot density as measured from GISAXS Fourier analysis are very close to the ex-situ values measured by AFM. The gallium nano-droplets was spontaneously generated by depositing a flux of Gallium by the MBE process on to sapphire, and finally converted to GaN by exposure to active nitrogen [27-28]. The formation of Gallium Nitride, as described by Moustakas et al

[24] occurs through the saturation of the gallium metal with the arriving active nitrogen, and this process is closer to a liquid phase process than a vapor phase process. In this paper we have investigated the growth of AlN under excess Al flux, which remained on the growth surface during deposition. The thickness of this metallic layer depends on both the flux employed as well as the time of deposition. The substrate temperature is not expected to play a major role, as the evaporation rate of Al is small under these conditions.

The conversion of Al metallic layer to AlN was carried out by intermittent closure of the metal shutter and exposure of the growth surface to active nitrogen exclusively. During this period, the RHEED was observed to change from a dim and diffuse to a clear and spotty pattern. This is shown in Fig 1, where the time periods for closure of the shutters are presented. Also, we show the time required for the RHEED to make the transition as described previously. During this exposure, it is expected that the Al nano-droplets formed on the growth surface will be completely converted to AlN nano-islands. Therefore, while standard droplet epitaxy process uses sequential arrivals of the group III and the group V elements, our modified process employs a group III-rich deposition process, followed by a purely group V exposure.

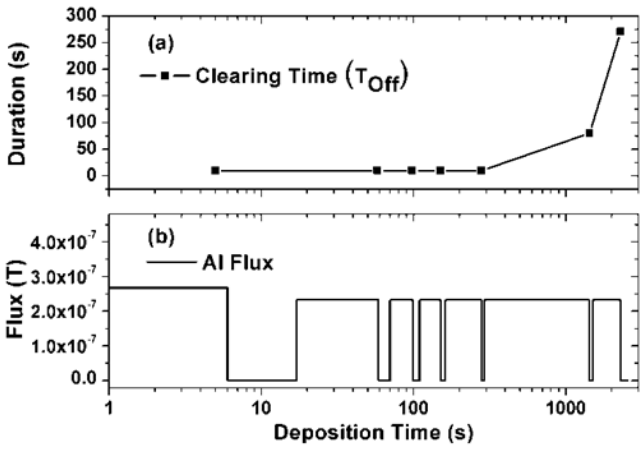

Figure 1: (a) Time taken for the RHEED screen to clear during AlN deposition (b) Aluminum flux used for the deposition of AlN

Subsequent to the growth of the AlN layer, an AlGaN layer was deposited with an Al flux of $1.08x10^{-7}$ T and a Gallium flux of $4.4x10^{-7}$ T, at similar substrate temperature and nitrogen plasma conditions. It should be noted that while the Al flux employed is significantly smaller than that employed in the AlN layer, it was about 75% of that required for stoichiometric growth of AlN. At this growth temperature, Gallium has significant desorption rate, which is not the case for Al. Nevertheless, the very excess Gallium causes the RHEED to go dim immediately, and this remains so during the growth process. Therefore, the Gallium metal layer builds on the growth surface, and is incorporated into the film by intermittent closure of the metal shutters, while the plasma shutter was kept open. The time of incorporation, as in the case of AlN, was determined by observation of the RHEED pattern, that is the transition from the dim and diffuse state to the clear and bright state. The last section of the AlGaN growth was carried out for 15 minutes, and the RHEED took as much as 120 seconds for the transition. The plasma was closed immediately after the transition of the RHEED pattern, so as to not cause any unintentional damage to the growth surface.

3. Results and Discussions

The schematic of the sample as described in the previous section is shown in the inset of Fig 2(a). The thicknesses of the AlN and AlGaN layers were found to be ~450nm and ~250nm respectively from cross-sectional SEM measurements. This gives a growth rate of about 17 monolayers per minute, which is close to the benchmarked value for growth under similar metal fluxes, plasma power, nitrogen flow rate and substrate temperature.

Post growth, the sample was studied by various characterization techniques to determine their morphological and optical properties. Photoluminescence measurements were carried out using a 10mW 224nm He-Ag laser, where the excitation was carried out from the top surface. Such an excitation is mostly attenuated within the top AlGaN layer, and does not reach the

AlN underneath, which in any case is not excited at these energies. The scattered luminescence from the laser is observed as a high-energy tail in the room temperature PL spectra, as shown in Fig 2(a). The PL spectrum shows a single peak at ~260nm, with negligible sub-bandgap luminescence. This is of importance because there have been many reports in the literature of PL spectrum with prominent deep level peaks, similar to the "yellow luminescence" in GaN [29-30]. The origin of these peaks can be either impurities incorporated during growth, or spontaneously generated point defects. The latter includes nitrogen vacancies and anti-site defects. There are also reports of deep level luminescence arising from presence of compositional inhomogeneities [31].

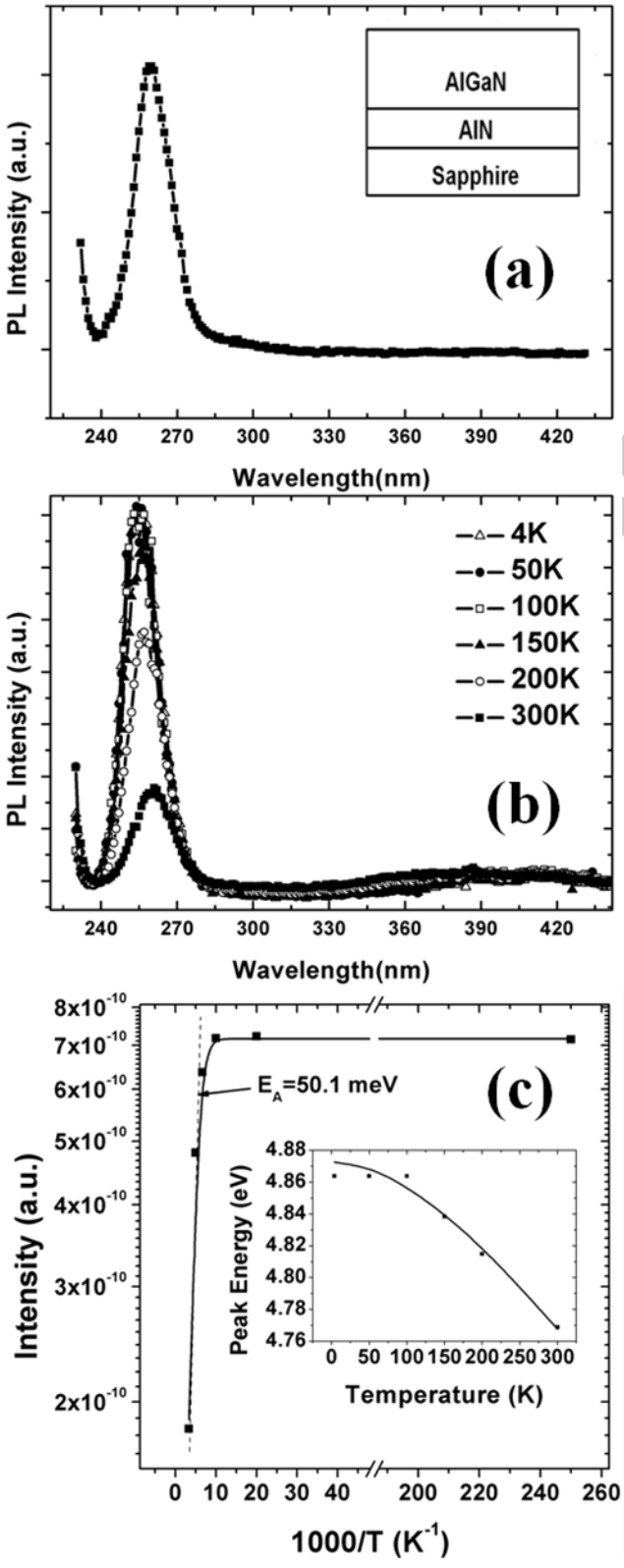

Figure 2: (a) Room Temperature PL spectrum (inset: Schematic of the grown structure), (b) Temperature dependent PL spectrum, (c) Plot of intensity with inverse of temperature (inset: Plot of peak energy with temperature fitted to the Varshni equation)

The absence of secondary peaks supports our RHEED observations that the material is of high quality, and is related in part to the typical low background impurity levels for MBE growth. The absence of nitrogen vacancies can also be related to the relatively low growth temperature compared to those used in MOCVD. An additional factor in PA-MBE is the power of the RF plasma, which can create highly energetic species, thereby creating damage to the material. An inference can be made that the frequent exposure of the growth surface to the nitrogen plasma does not create additional defects under the conditions - the plasma power - employed during this growth. The width of the PL peak at room temperature was ~17nm, which is broad compared to that typically observed for PA-MBE grown GaN. This broadening comes from various causes, the most important being the presence of disorder in the alloy. Bajaj et al has reported that the alloy broadening increases significantly for increased AlN content in AlGaN alloys, reaching a maximum around 80% [32]. The nominal AlN mole fraction in the alloy, as targeted, is around 75%, which accounts for the broad luminescence peak. Furthermore, the growth was carried out intentionally under extreme excess group III. It has been reported previously that under such conditions complex and possibly incommensurate long range atomic order may be present in the alloy [33]. This would also cause additional broadening of the peak.

Low temperature photoluminescence measurements were carried out down to 4K, and the results are presented in Fig 2(b). The nature of the spectrum remains the same, with no evolution of sharp deep level peaks, for the entire temperature range. The width also remains essentially unchanged, which is indicative that thermal broadening plays a relatively minor role compared to the other alloy-related phenomena. However a broad sub-bandgap luminescence was observed almost reaching the visible range which is relatively invariant with temperature. The main luminescence peak is however slightly asymmetric, which increases with decrease in temperature, and may be related to the presence of band-tails. The

peak energy has been plotted in the inset of 2(c) as a function of sample temperature, showing Varshni type dependence. This however saturates below 100K, which has been reported for AlGaN films and linked to the presence of compositional inhomogeneities in the alloy. The typical "S" type behaviour may be present in this case as well, which is not clear due to the wide spacing of the data. What is however more remarkable is the change in intensity with the cooldown. The intensity of the PL peak, which is due to excitonic transitions for these materials, increases with the decrease in temperature due to the increased stability of the exciton. The intensity ratio of the PL taken at room temperature to that taken at 4K has been linked to the internal quantum efficiency (IQE) of the PL process, which in most reported case is around 1% [34]. In our case however, it can be observed in Fig 2(c) that when the temperature is increased from 4K to 300K, the intensity decreased to about 25%. If this is linked to the IQE, a very high value would emerge, considering that this is from a bulk film of thickness less than 300nm, and therefore with high number of threading dislocations. Such increase in intensity is possible if the photo generated carriers are localized away from defects associated with dislocations, which would otherwise recombine non-radiatively.

The growth under high group III flux for both the AlN and the AlGaN and intermittent exposure to nitrogen plasma was carried out to generate nanostructures via the droplet epitaxy route, and the presence of nanostructures on the growth surface was investigated using FESEM. In a low magnification SEM image, as shown in Fig 3(a) the surface appears to be relatively flat and featureless. However, the flat regions are interspaced with areas of roughness, approximately of a circular nature around 10 µm in diameter. These areas appear to contain dense crystallite nuclei in this low magnification image, but upon further investigation shows an area completely populated with nanorod-like structures. These structures, as shown in Fig 3(b), are well oriented and vertical with average length ~500nm, even though some are as tall as nearly 1µm. Some of these taller nanorods can be observed to

be positioned parallel to the growth surface. It can be speculated that they were initially vertical, but have been dislocated from their original positions due to post growth handling. From plan view images, it was found that the cross-sections of the nanorods are very uniform, with a diameter about 250nm. The density of the nanostructures was estimated to be about 10^9 /cm^2.

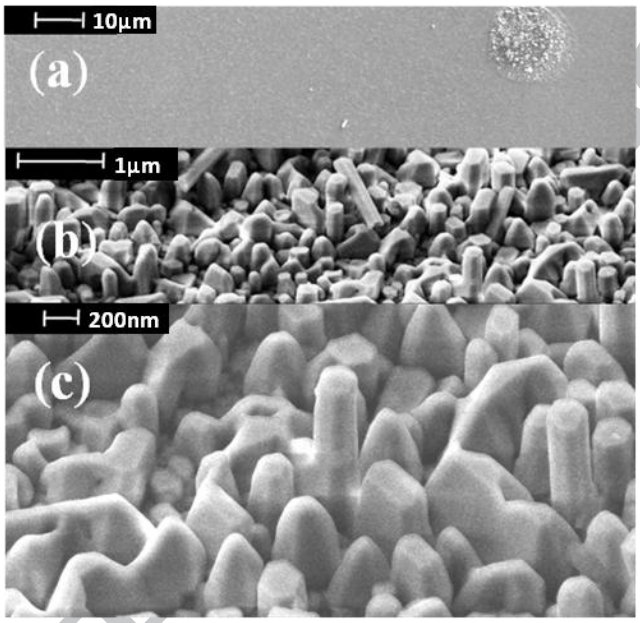

Figure 3: (a) SEM image of the surface at 10 µm scale (b) SEM image of the AlGaN nanorods at 1 µm scale (c) SEM image of the AlGaN nanorods at 200 nm scale

It is to be noted that the cross-section of the nanorods, as shown in high magnification in Fig 3(c) is clearly hexagonal, which along with the vertical orientation shows that the growth has taken place along the [0001] direction, as is expected from epitaxial deposition on to the (0001) plane sapphire substrate. It can also be observed that the various hexagonal rods are well aligned in-plane as well, with small degree of in-plane rotation. The nanorods were extracted using a Focussed-ion-beam based process, and were studied in the cross-section by TEM Selective Area Diffraction (TEM-SAD). These results, which are beyond the scope of this paper and will be reported elsewhere, also establish the c-plane orientation. Furthermore, the composition of exclusively the nanorods was obtained by cross-sectional TEM Energy

Dispersive X-ray Spectroscopy (TEM-EDX), and was found to be close to 98% AlN. These results indicate that the composition of the nanorods is close to that employed during the "buffer" layer initially deposited, and not the final AlGaN film. This, along with the length of the nanorods, shows that their initial nucleation happened during the initial phases of the deposition process.

It should be recalled that the Al flux employed during the initial deposition of AlN was deliberately kept significantly higher than that required for stoichiometric growth. As shown in Fig 1, after the growth of AlN layer using Al flux of about twice that required for stoichiometric growth, the film was kept under the nitrogen plasma for a period of 10 seconds. During this deposition, the excess metal stays on the surface, and accumulates with time. Due to two reasons, this excess metal is not expected to stay flat. First is the reduction of surface energy, and the second is the reduced surface diffusion of Al adatoms, specially at the growth temperature employed. Thus, a large density of nanoscale Al metallic droplets are formed on the growth front. During the period where the plasma is exclusively incident, these are converted into nano crystallites of AlN. Such structures are epitaxial, having been deposited on to sapphire after the nitridation process. However, their growth rate is expected to be significantly different from the rest of the film, which are grown by the traditional vapour phase growth. Again, both the materials are AlN, but one is grown by the usual MBE process, where the Al adatoms arrive on the substrate and react with active nitrogen, while the other is the dissolution of the active nitrogen into metallic nanoscale Al droplets already present on the growth surface. Subsequent growth of AlN enhances the difference between these two regions, till tall nanorods are formed with vertical orientation, which are epitaxial, but are generated from different origins. If a lower metallic flux was employed, the formation of the nanoscale Al droplets would have been avoided. On the other hand, if the active nitrogen was not made incident during intermittent growth, as described in Fig 1, the excess

metal would have remained on the growth surface un-reacted as a metallic layer and would have been observed even after deposition. Therefore, our deposition conditions are necessary for the formation of AlN nanorods by the phenomena of droplet-epitaxy.

Fig 3(a) indicates that the nanorods are not dispersed uniformly throughout the surface, but are localized within patches of roughly circular areas, which are about 10μm in diameter. We can postulate that the Al metallic regions, from which the nanostructures were generated, were originally dispersed in that fashion. This would of course depend on the substrate temperature, which determines the surface diffusion length of Aluminum. The interesting feature is that no GaN or high Gallium content AlGaN nanorods were observed during our studies, even though the top AlGaN layer was grown under very excess Gallium condition. During the AlGaN growth, the Al flux was only 75% of that required for complete reaction with the active nitrogen, therefore the question of excess Al does not arise. Therefore, it can be concluded that even though an excess Gallium metal was present on the surface, and the growth was intermittent as during the AlN film deposition, no AlGaN or GaN nanostructures were formed.

On investigating the surface at lower magnification, it was observed that the circular "patches" of AlN nanorods were not the only surface feature, but they were in reality part of much wider circular islands, being present at some cases at the exact center of these islands. This can be seen in the optical micrograph presented in Fig 4(a). The smallest dark spots indicated by "A", and about 10μm in diameter house the AlN nanorods as described before. Some of these islands are significantly large, indicated by "B" and are similar in the fact that they also house the AlN nanorods, but they are present at the center of larger circular features, which are sometimes concentric in nature. These features are indicated by "C" and they show one or more concentric alternate bright and dark rings ranging from 200μm to 600μm in diameter.

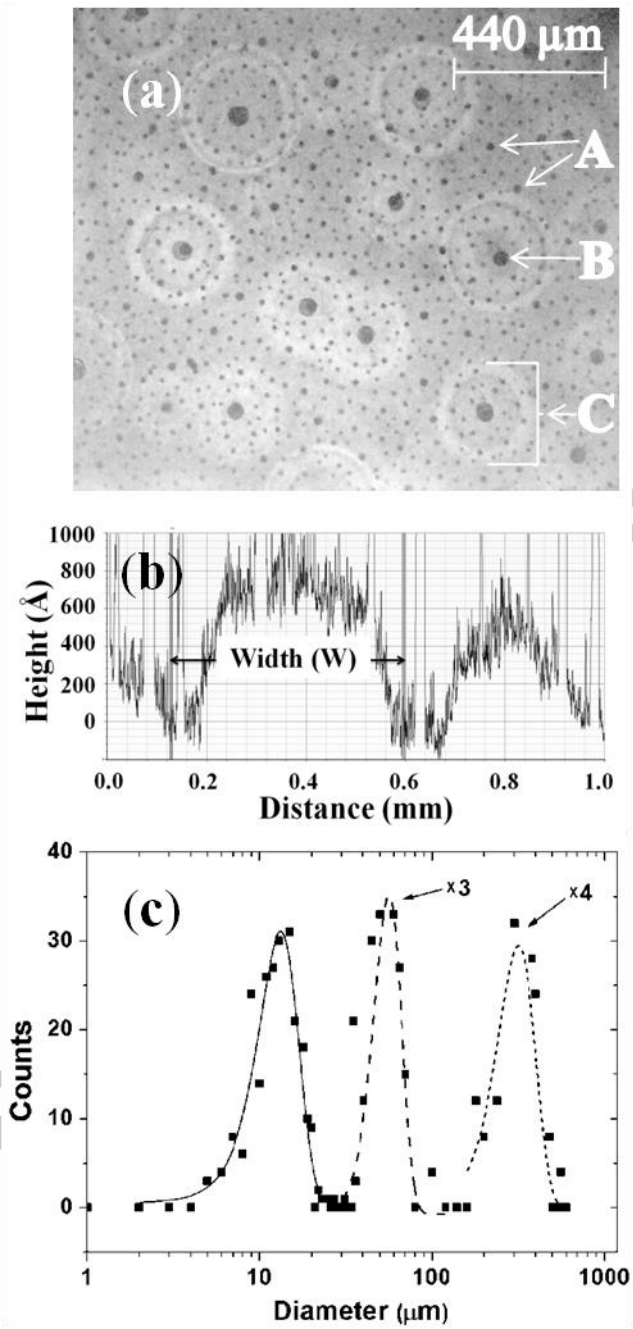

Figure 4: (a) Optical micrograph of the surface (b) Surface profilometer scan (c) Diameter distribution

The density of these various features has been plotted as a function of the diameters in Fig 4(c). The data reflects clearly that there is a very heterogeneous distribution of diameters, with the features A, B and C being clearly represented by three sharp and clear peaks centered at 10µm, 50µm and 400µm respectively. Therefore, it can be concluded that these

features have different origins, and were formed by different mechanisms during the growth process.

While the features A and B both have nearly AlN nanorods inside them, and thus were probably formed during the initial nucleation process, as discussed previously, the features C were probably formed during the AlGaN deposition. The features "C" observed in the optical micrograph can either be due to the variation of thickness leading to interference fringes, due to formation of regions of different compositions, or simply may be due to different surface morphologies, scattering light differently. In order to study the thickness of the film at the particular features, surface profilometry study was carried out, and the results are shown in Fig 4(b). While there are small variations, a typical feature observed in the optical micrograph with a diameter of 600µm, were found to be in reality a very flat dome like structure, with a height of 80nm at the center. Some of these features had a constant curvature, while others were mostly flat and reduced sharply near the edge.

It remains to be seen if these circular features, along with the variation of the thickness, also had any variation in alloy composition with the region in between them. EDX study was carried out in order to determine the spatial variation of Al, Ga and Nitrogen, and the results are presented in Fig 5. A specific region of the wafer surface was chosen for the measurement, which contained several complete circular features. In the SEM image, each of the two identical large features show a central region about 300µm in diameter, an inner circle about 75µm in diameter, a lighter region in the form of a ring about 40µm in width, and a final ring about 90µm in width, bringing the total diameter of the feature to ~600µm. One important question is if these features are due to metallic inclusions, which are simply excess metal being present on the growth surface. This was not the case, as seen from the Fig 5(d), which is the image of Nitrogen distribution in the film. The uniform distribution indicates that the film does not contain any un-reacted metal. This of course was ensured from the

RHEED image, which showed a clear pattern, not a diffuse one at the end of the growth, after the surface was exposed to the active nitrogen for a long period of time. This step consumed all the excess metal on the growth surface. It can be stated therefore that the two images, Fig 5(b) and 5(c) showing the distribution of Gallium and Aluminum, represent AlGaN alloys, and not metallic films.

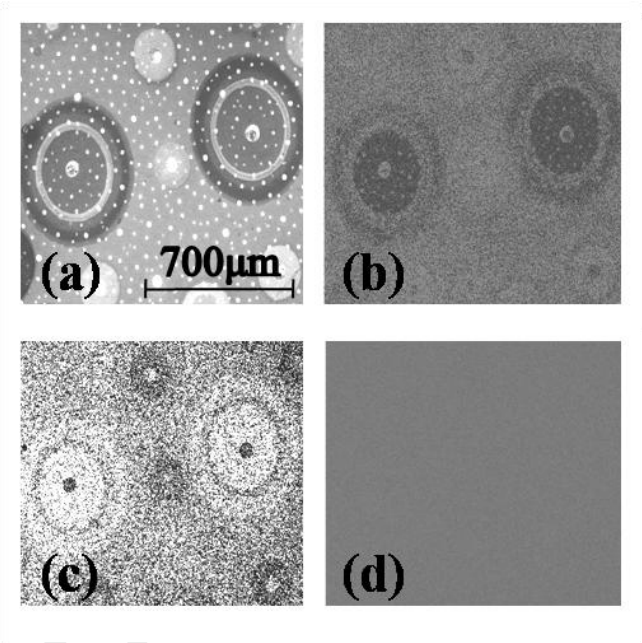

Figure 5: (a) SEM image of the surface; EDX profile for: (b) Gallium (c) Aluminum and (d) Nitrogen

In the EDX image shown in Fig 5(b) the Gallium composition is represented by the intensity distribution. We have already discussed the identical large features in the SEM image with its concentric rings. Here in the EDX image, similar rings corresponding to a variation of Gallium is clearly observed. The central region is bright, indicating a high Ga content. The adjacent circular region is darker followed by a brighter ring. The Ga content of this ring gradually decreases and merges with the outermost dark ring. It therefore shows a clear concentric variation of Gallium content in the AlGaN alloy. This data is perfectly correlated with Fig 5(c), the EDX image for Al that is the Al content in the AlGaN film. This image is

complimentary to that of Gallium, showing that the center is Al poor, and so it follows for the rest of the concentric rings.

Apart from the two large features, there are also smaller features present in the image. These also exhibit a concentric variation of Gallium and Aluminum content as with the larger features. However, it can be seen that the central position for these smaller features are similar for features of the same size, but opposite to that of bigger diameter. In addition, the smaller features have a lesser number of rings associated with them. Overall, a conclusion can be arrived at that the alloy composition for these features show a remarkable lateral fluctuation, which in reality has formed concentric in-plane heterostructures.

The formation of heterostructures has been already reported in AlGaN alloys [35-36], but the variation was not lateral, but along the vertical direction. The phenomenon of long range atomic ordering was observed by several groups, and for both InGaN and AlGaN alloys [37-39]. For extreme cases, such compositional fluctuations have led to the generation of spontaneous superlattices, of various periodicities [40]. Additionally, the phenomenon was closely linked to the group III to group V flux employed during growth, due to the difference in surface diffusion lengths of Gallium and Aluminum. Growth under group III rich conditions led to complex ordering which was found to be incommensurate with the crystal lattice [33], and therefore could only be explained in terms of the presence of a metallic adlayer on the growth surface, whose composition fluctuated with time. Growth by dissolution of active nitrogen into this film caused the composition fluctuation of the metallic film to be replicated in the AlGaN alloy composition. In our case, we believe a similar phenomenon has occurred, where the in-plane composition fluctuation of the metallic film on the growth surface during deposition of AlGaN layer was replicated in the alloy composition. Nanoscale in-plane compositional inhomogeneities have already been reported for AlGaN Multiple Quantum Wells (MQWs) [41]. Since the growth of bulk AlGaN in our case was

carried out for a longer time than for quantum structures, the metal accumulation is more enhanced, and the features reported in this work are significantly larger.

As to why we have a radial variation of the composition inside the circular features, there can be various reasons. The simple explanation could be in the difference of the diffusion lengths of Gallium and Aluminum ad-atoms on the growth surface at the time of deposition. This diffusion length has been linked to the mechanism of coarsening of the droplets during droplet epitaxy, and so similar effects can be present in our case. However that still does not explain the concentric variation where the region near the center of the feature as well as the edge of the feature has significantly higher Al content than the region in-between. It also cannot explain why for the larger features, the very center contains excess Gallium. We believe that this is related to two different mechanisms that happen during growth, that is the incorporation of active nitrogen into metallic droplets, and the desorption of the metallic layer due to high substrate temperature. The latter is much higher for Gallium than Aluminum under our conditions for deposition. Fig 6 shows the various steps that may lead to a concentric variation of composition.

We recall our previous understanding that the nanorods with composition close to AlN were formed during the initial deposition steps. Therefore, when the deposition of the AlGaN film was initiated the surface already contained these nanostructures at regular intervals. The AlGaN was grown with severely excess Gallium, which then formed a film on the growth surface, and unlike Aluminum the higher diffusion length did not allow the formation of GaN nanostructures. The metallic layer was uniform, and the thickness increased with deposition time. After a threshold thickness was reached, the surface formed large droplets due to minimization of surface energy, and this was present during the growth. When the interruptions happened, the surface was exposed to only the active nitrogen. A competitive process of several phenomena occurred at that time.

The first process is the shrinkage of the metallic droplets due to evaporation of Gallium now that the arrival rate was not present to keep up with the loss. The second was the in-plane diffusion of gallium to form larger, more spherical droplets in order to minimize surface energy. The third is the conversion of the metallic film to AlGaN by reaction with active nitrogen.

A schematic that shows the possible steps for these processes is presented in Fig 6. We have already stated that for the large AlGaN features, there is a central area that is filled with nearly AlN nanorods. This along with the fact that such nanorods were probably initiated during the nucleation, leads us to believe the largest circular features were necessarily formed around these nanostructures, either for energy minimization reasons, or that these nanorods locally modulate the desorption properties, increasing the sticking coefficient. This has been shown in Fig 6(a) where the nanostructures are present at the center of a metallic droplet, containing both gallium and aluminum. This is the situation at the end of the deposition process, when the metallic shutters are closed, and the plasma shutter is kept open.

During this period, two processes occur at the same time. The liquid metallic film, which have flat areas as well as droplets, go through uphill diffusion to reduce the surface energy and forms hemisphere-like droplets, with much smaller radius of curvature. The Gallium at the same time keeps desorbing, specially from the flat metallic layer, due to the higher surface to volume ratio. In other words, the flat areas disappear fast, while the rest of the material remains longer due to their spherical shape, as shown in Fig 6(b). During this process, simultaneously the active nitrogen keeps converting the metal to the III-Nitride semiconductor alloy. Now, since the mobility of the Gallium is much more than that of Aluminum, during this uphill diffusion process, the Aluminum gets left behind, and therefore converts into AlGaN forming the outer ring, which is richer in AlN (Fig 6(c)).

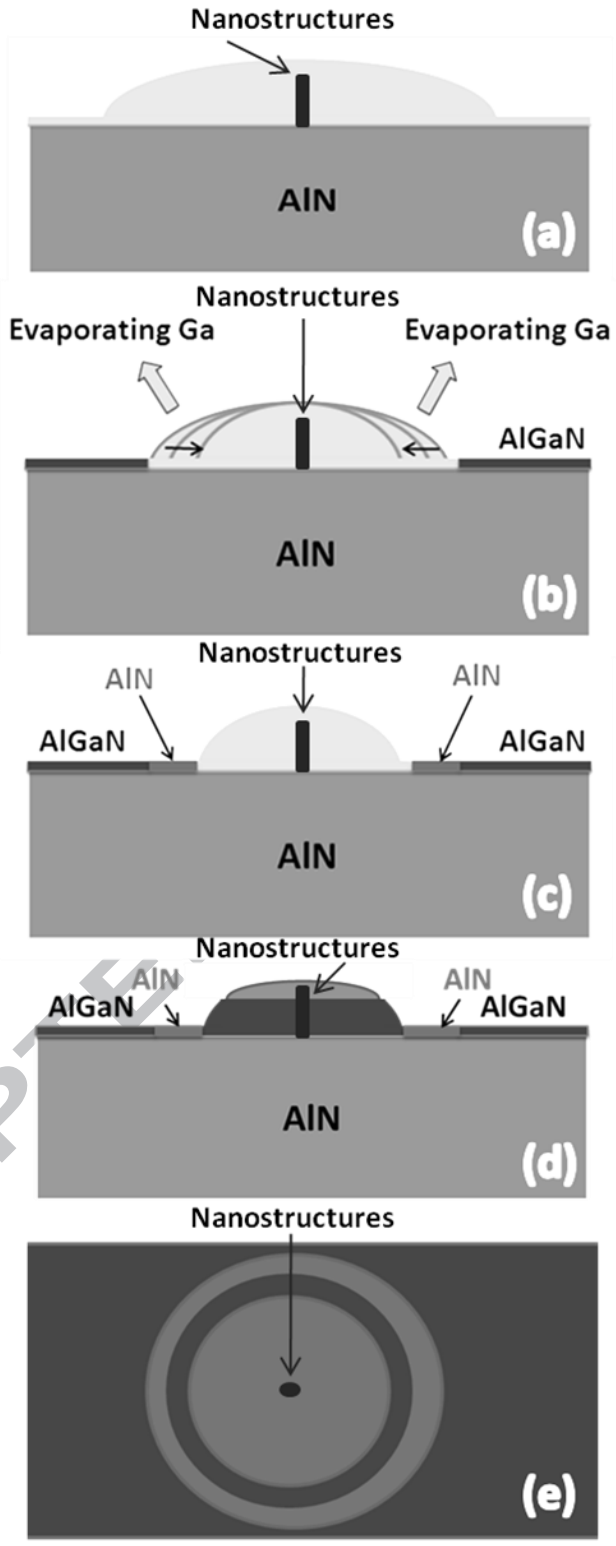

Figure 6: Schematic representing the steps of formation of the concentric circular features: (a) Metallic droplet formed around a region containing AlN nanorods, (b) Evaporation of Ga from the relatively flatter parts of the film, (c) Nitridation of the metallic film, (d) An inner ring is formed which is relatively richer in Ga as it is nitridated before the Ga can evaporate, (e) A top view of the final circular feature

Once the spherical droplets are formed, they keep evaporating and thereby reducing both in diameter and in height, while simultaneously converting into AlGaN. Since the desorption rate of Ga is faster, during the process, the droplets become progressively richer in Aluminum, but the alloy composition remains the same as it is given by the ratio of the Aluminum to the active nitrogen. This therefore forms the inner ring of AlGaN with relatively higher Gallium content (Fig 6(d)). After a certain time, the gallium mostly evaporates except for the region around the AlN nanorods, where as we speculated before, the desorption rate is much smaller. When Gallium is significantly reduced below the stoichiometric requirement, the AlGaN formed therefore becomes again rich with Al content. Thus, the inner high-Al content region is formed. Fig 6(e) shows the top view of the final feature formed. This is the mechanism for the formation of the lateral heterostructures shown in the EDX data. This of course depends on the size of the circular feature, which is also related to the volume of the metallic droplet that leads to its formation. In some cases, these features have merged together, showing that they might have been formed either at the same time, or at different times during the growth, because there were multiple interruptions during the growth of the AlGaN layer as shown in Fig 1(b).

4. Conclusions

In this work, we report on the formation of nanostructures of III-Nitride materials using a modified droplet epitaxy technique. Conventional droplet epitaxy is carried out by the deposition of metal films on the substrate, annealing to form nanoscale droplets and finally converting them to semiconductor nanostructures by exposure to active nitrogen plasma. We have on the other hand employed growth under excess group III conditions, with intermittent closing of the metal shutters and exposure to the active nitrogen. The results are remarkably different for AlN and AlGaN films.

For AlN, well oriented nanorods were formed by the droplet epitaxy process. They are vertical, epitaxial, and their cross-sections are very uniform at about 250nm. Their lengths range from 500nm to 1µm. For AlGaN on the other hand, there are no nanostructures formed even though the same intermittent growth at high group III was carried out. In its place, we observe truncated hemispheres with diameters up to 600µm and heights as small as 80nm. EDX studies show that these features are AlGaN with sharp concentric compositional variations. Spontaneous formation of radial heterostructures was observed under such conditions.

The variation is due the large difference in the surface diffusivity of the Al and Ga adatoms, specially at the growth temperature employed. For AlN, the reduced surface diffusion lengths of Al leads to formation of nanoscale metallic islands at the very initial steps. These get nitridated to form AlN nanostructures, which over the period of the growth form the well oriented vertical nanorods observed. For AlGaN however, the excess Gallium metal has very high diffusivity as well as desorption rates, and forms large islands, which during the exposure to active nitrogen mostly evaporates, leading to the reduced height of the truncated hemispheres. In the competition between evaporation, and nitridation, along with the necessity for minimization of surface energy, complex radial heterostructures were formed.

It has been already established in the literature that growth under excess group III enhances luminescence and quantum efficiencies, which has been postulated to be due to compositional inhomogeneities that lead to localization of carriers away from defect centers. These fluctuations are difficult to directly measure and have been observed indirectly by cathodoluminescence (CL) imaging showing a spatial variation of CL intensity [42]. In this work, we observe directly by EDX imaging the presence of lateral compositional fluctuation - in the form of spontaneous double heterostructures - that has been magnified by the extreme group III growth mode and preserved by the periodic exposure of the metallic layer to active

nitrogen. That this leads to an enhanced efficiency can be observed in the reduced variation of the PL intensity with lowering of temperature from 300K to 4K. Under controlled growth conditions, such phenomena can be utilized in increasing the efficiency of ultraviolet emitters.

Acknowledgements

This work was partially funded by the Department of Information Technology (12(3)/2011-PDD), Government of India. Chirantan Singha would like to acknowledge the Department of Science and Technology (DST) INSPIRE fellowship (IF120257), Sayantani Sen (09/028(0921)/2014-EMR-I), Pallabi Pramanik (09/028(0823)/2010-EMR-I) and Alakananda Das (09/028 (0946)/2015-EMR-I) would like to acknowledge the Council of Scientific and Industrial Research (CSIR) Senior Research Fellowship scheme and Mainak Palit would like to acknowledge World Bank TEQIP Phase-II for funding their work.

References

[1] M. L. Terranova, S. Orlanducci, M. Rossi and E. Tamburri, Nanoscale, (2015); doi: 10.1039/C4NR07171A.

[2] Eusebio Garate, Roger D. McWilliams, Donald E. Voss, Alexander L. Lovesee, Kyle J. Hendricks, Thomas A. Spencer, M. Collins Clark, and Amnon Fisher, Review of Scientific Instruments **66**, (1995) 2528; doi: 10.1063/1.1146504

[3] Jonathan J. Wierer, Jr, Aurelien David, Mischa M. Megens, Nature Photonics, **3 (**2009) 163-169; doi: 10.1038/nphoton.2009.21

[4] T. D. Moustakas, R. Paiella, Rep. Prog. Phys. **80** (2017) 106501; doi: 10.1088/1361-6633/aa7bb2

[5] Zhigang Zang, Xiaofeng Zeng, Jihe Du, Ming Wang, Xiaosheng Tang, Optics Letters, **41** (**15)** (2016) 3463; doi: 10.1364/OL.41.003463

[6] Y. B. Tang, H. T. Cong, Z. G. Zhao, and H. M. Cheng, Applied Physics Letters **86**, (2005) 153104; doi: 10.1063/1.1899763

[7] Jr Hau He, Rusen Yang, Yu Lun Chueh, Li Jen Chou, Lih Juann Chen, and Zhong Lin Wang, Adv. Mater. **18**, (2006), 650–654; doi: 10.1002/adma.200501803

[8] J.-M. Bonard, J.-P. Salvetat, T. Stöckli, L. Forr´o, A. Châtelain, Appl. Phys. A **69**, (1999) 245–254; doi: 10.1007/s003399900113

[9] J. Li, K. B. Nam, M. L. Nakarmi, J. Y. Lin, H. X. Jiang, Pierre Carrier and Su-Huai Wei, Appl. Phys. Lett. **83**, (2003) 5163; doi: 10.1063/1.1633965

[10] Renbing Wu, Kun Zhou, Jun Wei, Yizhong Huang, Fei Su, Jianjun Chen, and Liuying Wang, J. Phys. Chem. C **116**, (2012), 12940−12945; dx.doi.org/10.1021/jp3028935

[11] Qiang Wu, Zheng Hu, Xizhang Wang, Yinong Lu, Kaifu Huo, Shaozhi Deng, Ningsheng Xu, Bo Shen, Rong Zhang and Yi Chen, J. Mater. Chem., **13**, (2003), 2024–2027; doi: 10.1039/b303987k

[12] S. Zhao, A. T. Connie, M. H. T. Dastjerdi, X. H. Kong, Q. Wang, M. Djavid, S. Sadaf, X. D. Liu, I. Shih, H. Guo & Z. Mi, Scientific Reports **5**, (2015) 8332; doi: 10.1038/srep08332

[13] V. Cimalla, Ch. Foerster, D. Cengher, K. Tonisch, and O. Ambacher, phys. stat. sol. (b) **243** (7), (2006) 1476–1480; doi: 10.1002/pssb.200565205

[14] K.A. Bertness, A. Roshko, L.M. Mansfield, T.E. Harvey, N.A. Sanford, Journal of Crystal Growth **310**, (2008) 3154– 3158; doi: 10.1016/j.jcrysgro.2008.03.033

[15] I. N. Stranski and L. Krastanov, Sitzungsber. Akad. Wiss. Wien, Math.-Naturwiss. Kl., Abt. 2b **146**, (1938) 797; doi: 10/SWWCAS

[16] S. Varma, C.M. Reaves, V. Bressler-Hill, S.P. DenBaars, W.H. Weinberg, Surface Science **393**, (1997) 24-33; doi: https://doi.org/10.1016/S0039-6028(97)00231-8

[17] B. Daudin, F. Widmann, G. Feuillet, Y. Samson, M. Arlery, and J. L. Rouvie`re, Phys. Rev. B **56**, (1997) R7069(R); doi: https://doi.org/10.1103/PhysRevB.56.R7069

[18] Fereydoon Family, Paul Meakin, Phys Rev A Gen Phys. **40** (7), (1989), 3836-3854; doi: https://doi.org/10.1103/PhysRevA.40.3836

[19] Rachel A. Olivera, Haitham A.R. El-Ella, Daniel P. Collins, Benjamin Reid, Yucheng Zhang, Fiona Christie, Menno J. Kappers, Robert A. Taylor, Materials Science and Engineering B **178,** (2013) 1390– 1394; doi: http://dx.doi.org/10.1016/j.mseb.2013.08.011

[20] K.A. Bertnessa, A. Roshko, N.A. Sanford, J.M. Barker, A.V. Davydov, Journal of Crystal Growth **287**, (2006) 522–527; doi:10.1016/j.jcrysgro.2005.11.079

[21] A. V. Sampath, G. A. Garrett, R. W. Enck, P. Rottella, Jr., H. Shen, and M. Wraback, Journal of Vacuum Science & Technology B **29**, 03C134 (2011); doi: 10.1116/1.3585660

[22] T.D. Moustakas, E. Iliopoulos, A.V. Sampath, H.M. Ng, D. Doppalapudi, M. Misra, D. Korakakis, R. Singh, Journal of Crystal Growth **227** (2001) 13–20; doi: https://doi.org/10.1016/S0022-0248(01)00625-X

[23] Gon Namkoong, Elaissa Trybus, Kyung Keun Lee, Michael Moseley, W. Alan Doolittle, and David C. Look, Appl. Phys. Lett. **93**, (2008) 172112; doi: 10.1063/1.3005640

[24] T. D. Moustakas and A. Bhattacharyya, Phys. Status Solidi C **9**, (2012) 580; doi: 10.1002/pssc.201100427

[25] Pallabi Pramanik, Sayantani Sen, Chirantan Singha, Abhra Shankar Roy, Alakananda Das, Susanta Sen, and A. Bhattacharyya, Journal of Applied Physics **120**, (2016) 144502; doi: 10.1063/1.4964420

[26] J. M. Woodward, A. Yu. Nikiforov, K. F. Ludwig, T. D. Moustakas, Journal of Applied Physics **122** (2017) 065305; doi: 10.1063/1.4995429

[27] Yiyi Wang, Ahmet S. Özcan, Christopher Sanborn, Karl F. Ludwig, Anirban Bhattacharyya, Ramya Chandrasekaran, Theodore D. Moustakas, Lin Zhou and David J. Smith, J. Appl. Phys. **102**, (2007) 073522; doi: 10.1063/1.2786578

[28] Yiyi Wang, Ahmet S. Özcan, Karl F. Ludwig, Anirban Bhattacharyya, Journal of Applied Physics **103**, (2008) 103538; doi: 10.1063/1.2936969

[29] K. B. Nam, M. L. Nakarmi, J. Y. Lin, and H. X. Jiang, Appl. Phys. Lett. **86**, (2005) 222108; doi: 10.1063/1.1943489

[30] Jo¨rg Neugebauer and Chris G. Van de Walle, Appl. Phys. Lett. **69** (4), (1996); doi: http://dx.doi.org/10.1063/1.117767

[31] A. V. Sampath, G. A. Garrett, E.D. Readinger, R.W. Enck, H. Shen, M. Wraback, J. R. Grandusky, L. J. Schowalter, Solid-State Electronics. **54**, (2010) 1130–1134; doi: 10.1016/j.sse.2010.05.006

[32] Giuliano Coli, K. K. Bajaj, J. Li, J. Y. Lin, and H. X. Jiang, Appl. Phys. Lett. **80**, (2002) 2907; doi: 10.1063/1.1471932

[33] Yiyi Wang, Ahmet S. Özcan, Karl F. Ludwig, Jr., Anirban Bhattacharyya, T. D. Moustakas, Lin Zhou and David J. Smith, Appl. Phys. Lett. **88**, (2006) 181915; doi: 10.1063/1.2201898

[34] J. Mickevicˇius, G. Tamulaitis, M. Shur, M. Shatalov, J. Yang, and R. Gaska, Applied Physics Letters **101**, (2012) 211902; doi: 10.1063/1.4767657

[35] Pallabi Pramanik, Sayantani Sen, Chirantan Singha, Abhra Shankar Roy, Alakananda Das, Susanta Sen, Anirban Bhattacharyya, Deepak Kumar, D. V. Sridhara Rao, Journal of Crystal Growth **439**, (2016) 60–65; doi: http://dx.doi.org/10.1016/j.jcrysgro.2016.01.004

[36] J. P. Zhang, M. Asif Khan, W. H. Sun, H. M. Wang, C. Q. Chen, Q. Fareed, E. Kuokstis, and J. W. Yang, Appl. Phys. Lett. **81**, (2002) 4392; doi: 10.1063/1.1528726

[37] T. D. Moustakas, R. Singh, D. Korakakis, D. Doppalapudi, H.M. Ng, A. Sampath, E. Iliopoulos and M. Misra, Mat. Res. Soc. Symp. Proc. **482** (1998); doi: https://doi.org/10.1557/PROC-482-193

[38] E. Iliopoulos, K. F. Ludwig, Jr., T. D. Moustakas, S. N. G. Chu, Appl. Phys. Lett. **78**, (2001) 463; doi: http://doi.org/10.1063/1.1341222

[39] D. Doppalapudi, S. N. Basu, K. F. Ludwig, Jr. and T. D. Moustakas, Journal of Applied Physics **84**, (1998) 1389; doi: http://dx.doi.org/10.1063/1.368251

[40] Min Gao, S. T. Bradley, Yu Cao, D. Jena, Y. Lin, S. A. Ringel, J. Hwang, W. J. Schaff, L. J. Brillson, J. Appl. Phys. **100**, (2006) 103512; doi: http://dx.doi.org/10.1063/1.2382622

[41] Anand V. Sampath, Gregory A. Garrett, Ryan W. Enck, Paul Rotella, Jr., H. Shen, and Michael Wraback, Phys. Status Solidi C **8** (5), (2011) 1534–1538; doi: 10.1002/pssc.201001167

[42] Satoshi Kurai, Hideto Miyake, Kazumasa Hiramatsu and Yoichi Yamada, J. Appl. Phys. **119**, (2016) 025707; doi: http://dx.doi.org/10.1063/1.4939864

Highlights:

• III-Nitride nanostructures grown using a modified droplet epitaxy technique

• AlN uniform vertical nano-rods formed with length/width 1μ m / 250nm

• Spontaneous growth of radial AlGaN double heterostructures observed by EDX imaging

• AlGaN PL peak at 260nm reduces to 25% from 4K to 300K indicating high IQE